3D GPU SPH analysis of coupled sloshing and roll motion

Luis Pérez-Rojas, *CEHINAV, ETSIN, UPM, Madrid, Spain*, luis.perezrojas@upm.es

Jose L. Cercos-Pita, *CEHINAV, ETSIN, UPM, Madrid, Spain*, jl.cercos@upm.es

ABSTRACT

The coupled roll motion response of a single degree of freedom system to which a passive anti-roll tank has been attached is considered and its performance studied numerically with a 3D GPU SPH code, aimed at simulating the sloshing flows occurring inside the tank. Results are compared with experiments from [Bulian et al, *JHR , 48, 2010*] in which 2D simulations were also presented. Progress achieved thereafter is documented, mainly consisting in the implementation of a parallelized solver that runs on a GPU card, which allows the simulation of low resolution 3D and high resolution 2D computations.

Keywords: *SPH, antiroll tanks, single degree of freedom systems, SDOF, GPU, sloshing*

1. INTRODUCTION

Ship motions are affected by sloshing flows occurring inside her liquid cargo tanks, as has already been documented both numerically and experimentally in the literature. Nam et al. (2009) for instance, use a finite difference method to model the flow inside the tanks and a linear sea-keeping code for the vessel motions simulation. A multimodal approach to sloshing presents large problems in resonance condition due to the lack of an intrinsic dissipation mechanism. Mesh based simulation techniques often struggle with sloshing flows due to the tremendous fragmentation that takes place at the free surface in resonance conditions. Due to this, meshless methods like SPH become an attractive option to simulate these flows, albeit to tackle 6 degrees of freedom, a full 3D SPH solver is necessary.

The onset of sloshing flows inside tanks has been used in order to dampen the roll motion. The antiroll tank concept is equivalent to the tuned sloshing damper or tuned liquid damper (TLD) concept in Civil Engineering. In the existing literature, two approaches can be found to characterise the behaviour of a TLD exposed to external excitations. The first one consists in imposing a periodic motion on the TLD by using a shaking table or a forced roll motion device and measuring the response in terms of lateral force or moment (Tait et al., 2005; Souto-Iglesias et al. 2006). The other approach, more complex, and the one the present paper deals with, is to consider the motion response of the coupled system and tank-structure, subjected to external excitation in terms of force, moment or even induced motion to the tank interfaced with an elastic structure. With this second approach the damping characteristics, inertia and restoring terms are also relevant in the dynamic analysis. Realistic motions of the structure that are the outcome of this process can be compared with design limit states (Bulian et al, 2010; Attari and Rofooei, 2008).

In this paper, the SDOF system of (Bulian et al, 2010), to which a partially filled tank has been attached is considered. The roll motion is modelled by means of an "exact" (from the dynamics point of view) 1-DOF approach. The moment created by the fluid with respect to the rolling axis is simulated and results for different roll angles are compared. It is

important to underline that the present experimental/numerical approach removes the difficulties usually encountered in a correct modelling of the actual ship roll motion. Indeed, when numerical simulations are compared with experimental tests carried out on ship models excited by waves, it is almost never completely clear where the real source of discrepancy between experimental results and numerical prediction comes from, i.e. whether the reason is to be sought in the modelling of sea-ship interaction or in the modelling of sea-tank interaction. In the present tests, being the dynamics of the mechanical system practically known "exactly" (at least at a reasonable level of accuracy, with some question mark on damping at small rolling angles), any significant discrepancy is likely to be sought in the simulation method.

The numerical simulations have been performed using the SPH particle method. SPH has been successfully applied to shallow depth sloshing problems with periodic oscillation in sway (Landrini et al. 2003) and roll (Souto et.al., 2006) motions. It had also been applied to a coupled motion problem (Bulian et al, 2010), showing promising results. Nevertheless, in (Bulian et al, 2010), the computations were carried out in 2D whilst 3D computations are presented herein. A significant progress in this regard has been recently achieved through the use of graphical cards (GPUs) that can perform massive parallel SPH computations (Herault et al, 2010, Rey-Villaverde et al., 2011). These cards are extremely cheap and incorporate of the order of 500 processors each, substantially speeding up SPH computations. It would be extremely interesting to obtain an accurate description of the effect of the flow inside the tank to the system using a GPU based SPH solver, since SPH is, in principle, able to deal with highly distorted free surface flows. Checking whether this is feasible is the main objective of the present work.

The paper is organized as follows. Firstly, the experiments are briefly described. Secondly, the GPU based SPH implementation is described. Thirdly, the simulation results are presented and compared with the experimental ones. Finally, some conclusions are drawn and future work threads hinted.

2. EXPERIMENTS AND MECHANICAL MODEL.

2.1 Experiments.

The experiments were conducted with the tank testing device of the CEHINAV group (see Souto-Iglesias et al 2011 for a detailed description). The standard forced motion configuration of the device, used regularly in the design of anti-roll tanks, was modified by disconnecting the driving electrical engine from the tank holding structure, in order to allow a free motion of the tank.

The tank is rectangular, 900x508x62mm. A horizontal linear guide consisting of a controllable electrical engine that laterally moves a weight with a specified motion has been attached. This weight is intended to generate a heeling moment in order to reproduce the wave action on the roll motion.

The water depth (H) whose first sloshing frequency matches the first own frequency of the structural system ω_0 (3.26 rad/s) has been chosen for the experiments and the same frequency has been chosen for the weight movement. This resonance condition is the hardest to tackle since in this condition the system accumulates energy in every cycle which then has to be dissipated by the fluid through internal dissipation and breaking in order to reach a steady state condition.

The amplitude of the weight motion has been chosen as A=100 mm. This combination of frequency and amplitude were the ones analyzed in greater detail in (Bulian et al, 2010). Three different liquids have been used, namely: water, sunflower oil and glycerin, covering 3 different orders of Reynolds

numbers. In the case of water, the dissipation comes from breaking and internal dissipation while the larger viscosity of oil and glycerine does not allow such breaking to take place thus inducing much smaller dampening effects than water. The experiments have been considered relevant by the SPHERIC ERCOFTAC Interest group on SPH as a benchmark for validation and further information about the experimental data can be found in the SPHERIC site and in (Bulian et al, 2010).

2.2 Analytical Model of the system.

An analytical model of the SDOF structural system used in the experiments is needed in order to incorporate it into the structural part of the SPH code. This model was obtained by deducing the coefficients after carefully analyzing a set of tests with the empty tank and deriving a data-consistent damping term model. The analytical model used to describe the behaviour of the system is, in general, as follows:

$$\left[I_o + m\,\xi_m^2(t)\right]\cdot\ddot{\phi} + 2m\,\xi_m(t)\,\dot{\xi}_m(t)\cdot\dot{\phi} - g\cdot S_G\cdot\sin(\phi) + m\cdot g\cdot\xi_m(t)\cdot\cos(\phi) = Q_{damp}(t) + Q_{fluid}(t) \quad (1)$$

$$Q_{damp}(t) = -K_{df}\cdot sign\left(\dot{\phi}\right) - B_\phi\cdot\dot{\phi} \quad (2)$$

where:

- ϕ [rad] is the roll angle.
- g $[m/s^2]$ is the gravitational acceleration.
- I_o $[kg\cdot m^2]$ is the polar moment of inertia of the rigid system.
- m $[kg]$ is the mass of the moving weight.
- $\xi_m(t)$ [m] is the instantaneous (imposed) position of the excitation weight along the linear guide (tank-fixed reference system).
- $\dot{\xi}_m(t)$ [m/s] time derivative of $\xi_m(t)$ [m].
- $S_G = M_R\cdot\eta_G$ $[kg\cdot m]$ is the static moment of the rigid system with respect to the rotation axis.
- M_R[kg] is the total mass of the rigid system.
- η_G [m] is the(signed) distance of the centre of gravity of the rigid system with respect to the rotation axis (tank-fixed reference system).
- $Q_{damp}(t) = -K_{df}\cdot sign\left(\dot{\phi}\right) - B_\phi\cdot\dot{\phi}$ $[N\cdot m]$ is the assumed form of roll damping moment with a:
- A dry friction term $-K_{df}\cdot sign\left(\dot{\phi}\right)$ with K_{df} $[N\cdot m]$ being the dry friction coefficient.
- A linear damping term $-B_\phi\cdot\dot{\phi}$ with
- B_ϕ $[N\cdot m/(rad/s)]$ being the linear damping coefficient.
- $Q_{fluid}(t)$ $[N\cdot m]$ is the fluid moment.

By using a set of inclining as well as decay tests, the unknown parameters have been experimentally determined, including the natural frequency of the rigid system ω_0. The values of these parameters can be found in table 1.

Quantity	Units	Value
S_G	$kg\cdot m$	-29.2
I_o	$kg\cdot m^2$	26.9
K_{df}	$N\cdot m$	0.540
B_ϕ	$N\cdot m/(rad/s)$	0.326
ω_0	rad/s	3.26

Table 1: Mechanical parameters of the rigid system

2.3 Dissipation indicator

The rotating mechanical system stores energy in kinetic and potential forms. There is a transfer between these forms of energy during each rotation cycle. This accumulation is significantly reduced with the fluid action, which dissipates part of that energy in every cycle. Since the potential energy is proportional to the square of the rotation angle amplitude, a reasonable indicator of the TLD dampening performance is defined as the ratio of the empty tank motion amplitude and the partially filled tank motion amplitude, as in (Bulian et al., 2010).

3. GPU-SPH FORMULATION

3.1 General

The recent implantation of graphic process units (GPUs) in scientific computation has drastically increased the processing speed of several applications. Not many years ago, parallel computing was restricted to super-computing centers or large and expensive clusters. Nowadays, thanks to the arrival of GPU multicore processors originally designed for graphic processing, massively parallel processing is becoming increasingly more accessible and cheaper for the developer.

Increasing the efficiency of the algorithms involved not only depends on the specific hardware improvements, but also on the new approaches aimed at maximizing available resources and minimizing costs. In the case of GPU processors, it is necessary to note that the computational power lies in its specialization. The GPU multicore architecture is designed for highly efficient graphic processing. To explore the degree of adaptability of the GPU technology to certain algorithms which simulate large particle systems, first we analyze which steps of the SPH (Smoothed Particle Hydrodynamics) code are more suitable to be parallelized, as well as different strategies for the parallelization of the main subroutines. This requires the evaluation of any problematic aspect and the consequent speedup and scalability obtained.

Since the SPH methodology generally uses an explicit resolution scheme, their algorithms are easily parallelized to its minimum unit (particles, cells). However, there are certain subroutines whose GPU parallelization is not immediate; in those cases, different strategies will be implemented focusing on obtaining the maximum increase of the CPU versatility. Although it is always possible to use the CPU in those subroutines whose parallelization is problematic, this should be avoided due to the relatively high latencies associated with data transfers between CPU and GPU and the consequent reductions in computational performance.

3.2 GP-GPU: OPEN CL implementation

Traditionally, the GP-GPU has been developed using special languages (shaders) as GLSL, CG, or HLSL and incorporated as extensions of the OpenGL and Direct3D APIs. Learning GP-GPU programming not only required graphic programming as a prerequisite, but also required a considerable expertise in APIs and graphic languages. Currently, developing GP-GPU applications is done with the help of programming environments specifically designed to develop this type of codes such as the CUDA or OpenCL platforms.

Regarding the GPU architecture, a scheme of the processors distribution in the graphic cards used, is shown in figure 1. Basically, the GPU is distributed in a set of multiprocessors. Each multiprocessor typically hosts 8 scalar processors with NVIDIA architectures. From the viewpoint of parallel codes, the first important concept to consider is related to the kernel functions (analogous to the shaders in the graphic computing context). When a kernel is called, it launches a vector of N threads where each thread is executed in a different processor. In turn, every thread executes the instructions found in the kernel function sequentially. Once the kernel function is called, the N threads perform the instructions in parallel. Threads are grouped into blocks of threads. The threads associated in a specific block are executed in a common multiprocessor (8 single processors) where they can share variables and make use of the shared memory space associated to each multiprocessor.

When a kernel is called, blocks of threads are listed and distributed in the available multiprocessors. The threads of a block are executed simultaneously on a single multiprocessor, while multiple blocks could be executed concurrently in one multiprocessor.

Once all the threads of a block have been processed, new blocks are launched in the vacant multiprocessors. One multiprocessor can concurrently execute hundreds of threads. To efficiently manage the large number of threads, it uses a special architecture called SIMT (Single Instruction, Multiple Thread). The total amount of threads is divided into 32 unit packs called warps. In the SIMT architecture, the threads of a warp execute the same kernel instruction at the same time. In order to make a parallel implementation, achieve maximum transfer rates and avoid bottlenecks, it is crucial to understand the GPU memory hierarchy in order to manage different memory spaces .

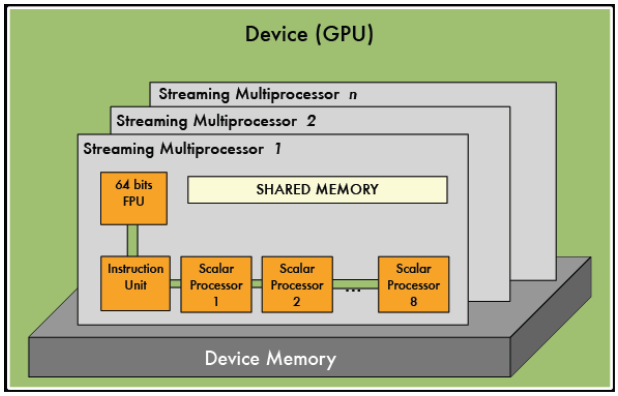

Figure 1 Basic architecture of a GPU card.

3.3 SPH parallel code.

Smoothed Particle Hydrodynamics (SPH) is a Lagrangian method, with no computational mesh that has been widely employed to study free-surface flows (Monaghan, 1994). A recent comprehensive review can be found in (Monaghan, 2005).

Due to the large number of interactions for each particle at each time step, when SPH codes are computed on a single CPU they usually require a large computational time. When millions of particles are required to accurately compute a physical process, only a parallel computing setup can guarantee efficient computational times. Due to the inexorable development of the market of video games and multimedia, the GPU power and streaming multi-processor technology has increased much faster than CPUs. Thus, GPUs now appear as an accessible alternative to accelerate SPH models using a powerful parallel programming model where the graphics cards are used as the execution device. Their performance can be compared with large cluster machines. A huge advantage is the price and the easy maintenance GPUs require in comparison with large multi-core systems. The capability of GPUs to handle SPH was shown by the pioneer work of Harada et al. (2007).

A weakly compressible SPH implementation has been chosen for the simulations, using a Wendland kernel, a second order Leap-Frog time integration scheme and Monaghan, Cleary and Gingold's (Monaghan et al., 1983) viscosity formula (MCG formula from now on). The no-slip boundary condition is simulated using several rows of fixed fluid particles attached to the solid boundary (Macià et al., 2011). Although we kindly refer the reader to (Souto-Iglesias et al., 2006, Rey-Villaverde et al., 2011) for further details on the GPU-SPH implementation used in the present work, let's point out some details about its dissipation mechanisms.

In (Colagrossi et al., 2011) it was demonstrated that in the continuum, MCG viscosity formula provides the correct viscous dissipation for free surface flows. This viscosity formulation was originally devised as an artificial viscosity but was later shown to be a consistent Newtonian viscous term for incompressible flows (Hu and Adams, 2006). When comparing the kinematic viscosity with the artificial viscosity, the following relation is obtained in 2D and an equivalent one with a denominator of 15 in 3D:

$$\nu = \frac{1}{8}\alpha h c_s \qquad (1)$$

The α factor should be no less than 0.01 if time integration is expected to remain stable (Monaghan 1994), with c_s being 10 times the

maximum expected velocity and *h* the smoothing length. This link sets the minimum value of the kinematic viscosity for a certain resolution (keep in mind that in practical terms the typical particle distance Δx is proportional to *h*). Since the computational effort was limited to 2 days per case (around 3e5 particles), it was not feasible to perform a full resolution 3D computation for the water and oil cases.

4. RESULTS

4.1 General

In order to limit the computational effort, the simulations have been run up to 30 seconds (~15 oscillation cycles). Results are presented in terms of the angle across the time history and comparing experimental with simulation results for each fluid. Free surface shape results are also presented.

4.2 Glycerin

For the glycerin case, the fluid adheres to the walls of the tank due to its large dynamic viscosity (0.934 Pa/s, around 1000 times larger than water). Therefore, the effect of the front and aft walls may have an effect in the simulations when comparing the 3D with the 2D case. The stability criterion of equation 1 is fulfilled for the 3D simulation with 300,000 particles. The maximum experimental angle after 30 seconds is 17 degrees, while the 2D simulation angle only reaches 7 degrees (figure 2). This is a consequence of the dissipation being much larger in the 2D simulation compared to the experiments due to the absence of the front and aft wall boundary layers. Therefore in this case the 2D hypothesis is not acceptable.

The 3D simulation result is much closer to the experimental one (13 degrees compared to 17 in the experiments) although identifying the origin of the discrepancies requires further research work. In both the 2D and 3D simulations there is a slight lag compared to the experimental result.

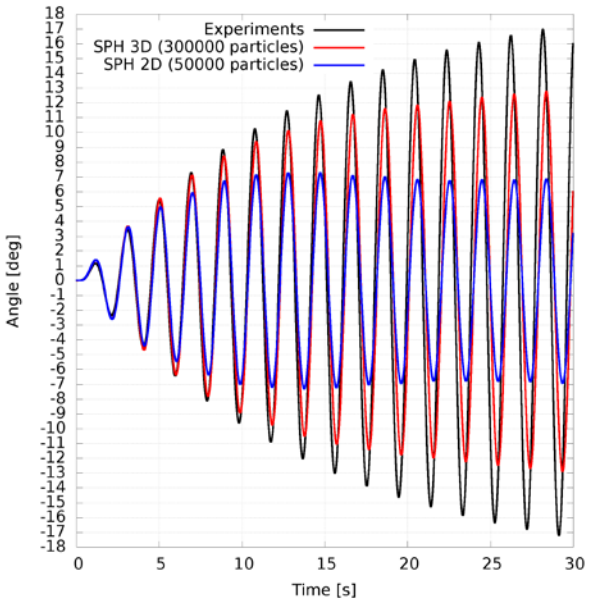

Figure 2 Glycerin case roll angle

4.3 Oil

The 2D case can be run at full resolution in regards to correctly modelling the dynamic viscosity of the fluid (0.045 Pa/s) by using 200,000 particles. Around 5 million particles would be necessary to run a 3D case and this was not possible at this stage due to the time necessary to obtain a reasonable estimation of the damping effect (30 seconds).

The maximum experimental angle was 12 degrees, while the maximum angle in the 2D simulation was 10 degrees. The accuracy is therefore reasonable. The time history of the experiments and simulations can be appreciated in figure 3. In the simulation there is a slight lag compared to the experimental result.

4.4 Water

The effective viscosity that can be reached for this case with 100,000 particles in 2D was 0.068114 Pa/s, more than one order of magnitude larger than real water viscosity and

quite similar to oil. It was therefore not possible to run a 3D simulation. In the water case, the influence of both the front and back walls is negligible and the 2D approximation should therefore provide reasonable results.

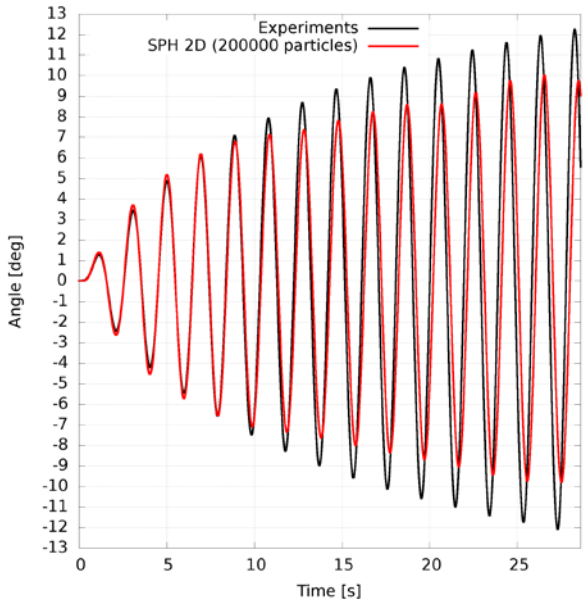

Figure 3 Oil case roll angle.

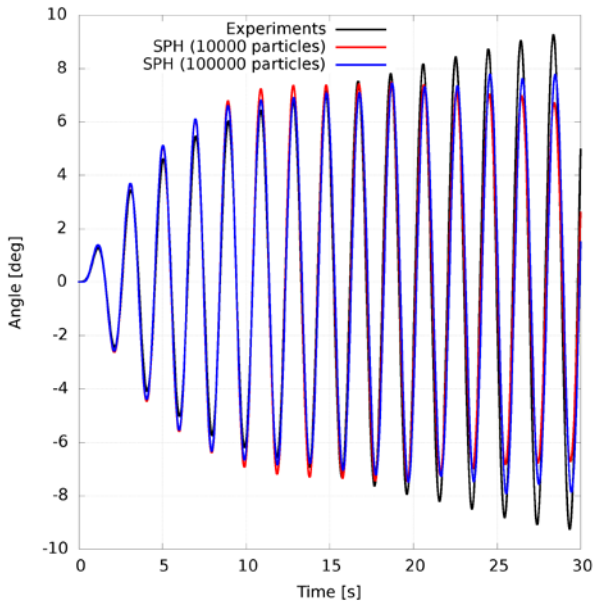

Figure 4 Water results

The maximum experimental angle was 9.5 degrees, while the maximum angle in the 2D simulation was 7.9 degrees. The accuracy is therefore reasonable. The time history of the experiments and simulations can be appreciated in figure 4 where two resolutions results are presented. In the simulation, no lag is present compared to the experimental result.

4.5 Free surface shape

Together with the roll angle time history it is relevant to analyze the free surface evolution for each case. In figure 5, the free surface is presented for the 2D simulations of the three liquids when t=9.43s (t/T_0=4.9, T_0 being the first sloshing period). In this instant the tank is in its horizontal position for the water case while there is a slight deviation from this position for the oil and a more significant one for the glycerin case. The free surface pattern is quite different for the glycerin as compared to the water and oil cases, for which, as already discussed, the effective numerical viscosity was finally similar for this resolution. The glycerine shape is single valued while a breaking wave is observed in the oil case and the building up of a breaking wave can be appreciated for the water case.

As the simulation evolves to a point of extreme roll angle (t=10s, t/T_0=5.2, figure 6), a strong wave run-up with overturning waves and breaking takes place for the oil and the water simulations while a mild run-up occurs for the glycerin. The matching of these cases with the experiments can be observed by comparing figure 6 with figures 7 and 9.

The objective of the present paper is to assess the capabilities of SPH to deal with full 3D flows coupling problems in resonance conditions, where attenuating the vessel motion by dissipating energy through sloshing is the main target. 3D Results of the computations with glycerin are presented in figures 8 and 9. As discussed in section 4.2, the 2D simulation presents a much larger dissipation than the experimental one due to the absence of the effect of the back and front walls of the container. If the free surface shape of the glycerin in 2D for t=9.43s in figure 5 is compared with the 3D one in figure 8, the matching with the experiments is much better for the 3D case, which is coherent with the roll

angle found for both cases, as presented in figure 2. This tendency is confirmed by looking at the t=10s frames. In the 2D simulation shown in figure 6, a mild but significant wave run-up is apparent. This is not the case in 3D as can be seen in both the experiments and 3D simulations (figure 9).

Another interesting feature that can be observed in figures 8 and 9, is how the fluid sticks to the wall in both the simulations and experiments, thus confirming the importance of the front and back walls of the container in flow dynamics.

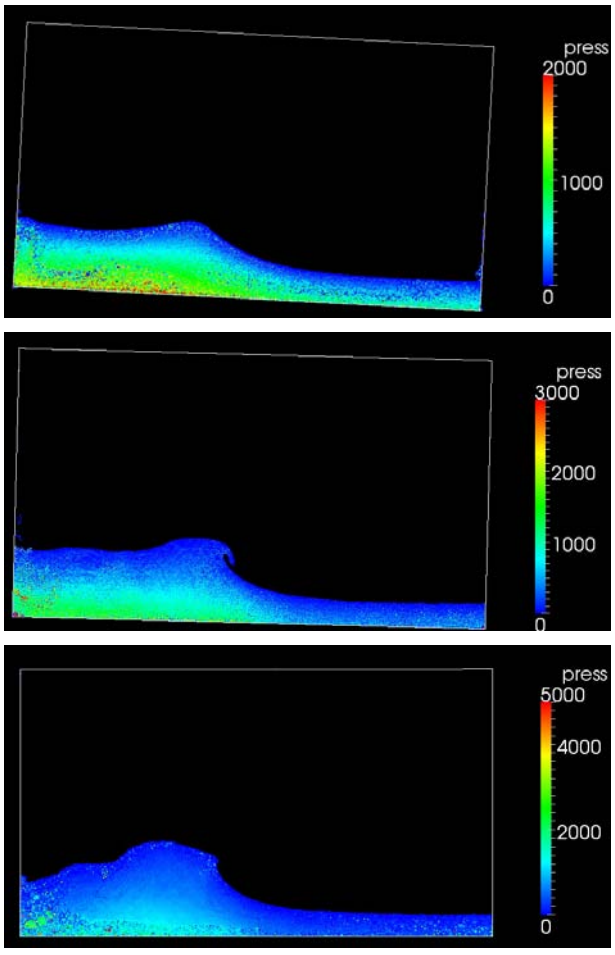

Figure 5 Glycerin (top), oil (mid), water (bottom), t=9.43s

5. CONCLUSIONS

The roll motion response of a single degree of freedom (SDOF) structural system for which an "exact" analytic mechanical model is available and to which a rigid rectangular partially filled liquid tank was attached has been considered. The coupled sloshing and SDOF system motion in resonance conditions has been numerically studied with a 3D GUP based SPH model and compared with the experimental results.

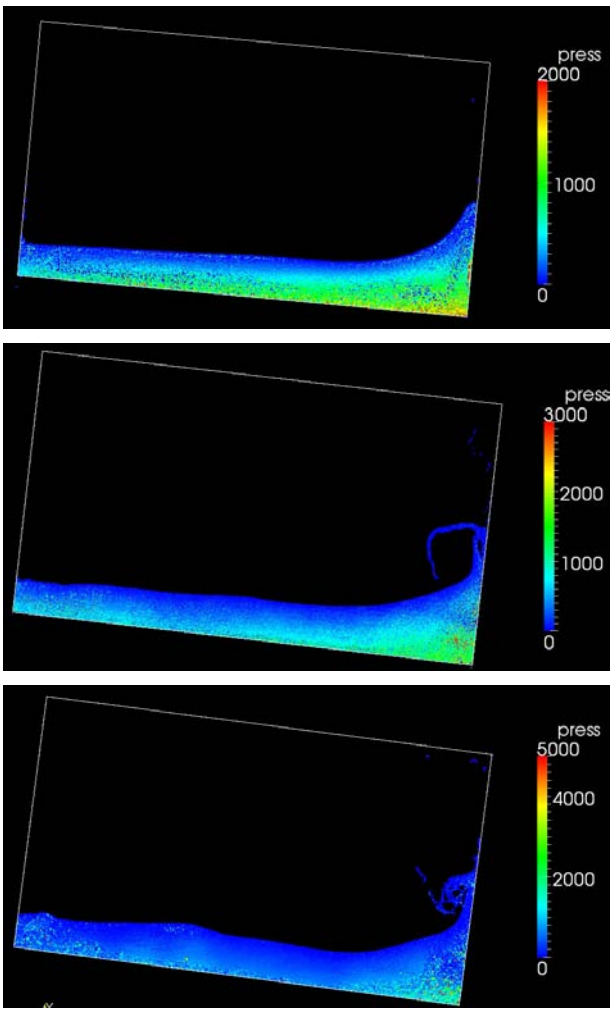

Figure 6 Glycerin (top), oil (mid), water (bottom), t=10s

In order to characterise the type flow dynamics effects on the response curves, simulations have been performed with liquids of different viscosity, concluding that increasing the viscosity prevents the onset of breaking waves. The capabilities of SPH to treat this coupling problem have been assessed. From the comparisons with the experiments, it seems that SPH is able to capture part of the dissipation effects due to wave breaking which

is reflected in reasonably accurate damping reduction ratios. Nevertheless, there are intrinsic limitations in the stability of the method that limit the effective Reynolds number which can be reached for a certain resolution. Further work has to be done in this regard.

The next step along this path is to incorporate the SPH model of the tanks internal flow into a 6DOF ship motions model.

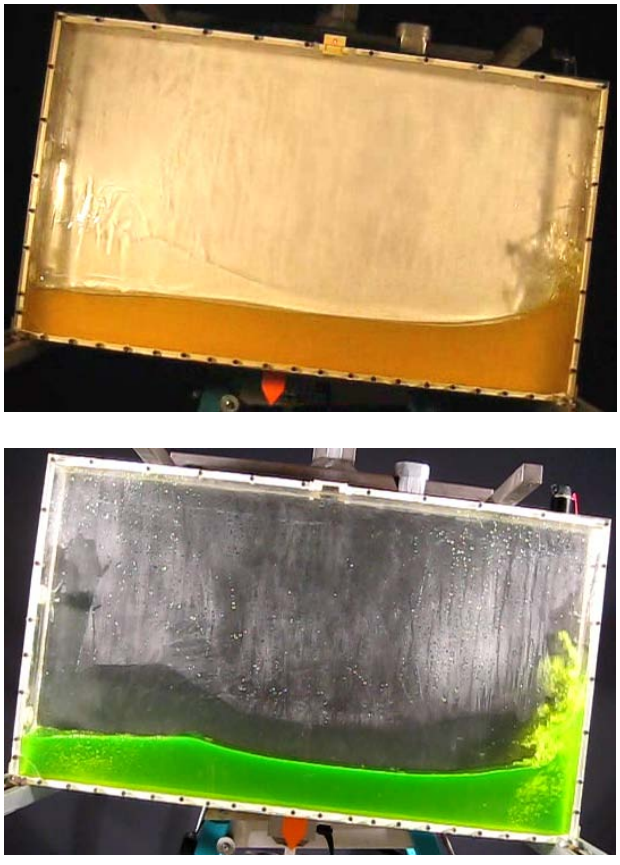

Figure 7 Experiments, oil (top), water (mid), t=10s

6. ACKNOWLEDGEMENTS

The research leading to these results has received funding from the Spanish Ministry for Science and Innovation under grant TRA2010-16988, "Caracterización Numérica y Experimental de las Cargas Fluido-Dinámicas en el transporte de Gas Licuado".

7. REFERENCES

Attari, N.K.A., Rofooei, F.R., 2008, "On lateral response of structures containing a cylindrical liquid tank under the effect of fluid/structure resonances", Journal of Sound and Vibration, 318, 4-5, 1154-1179

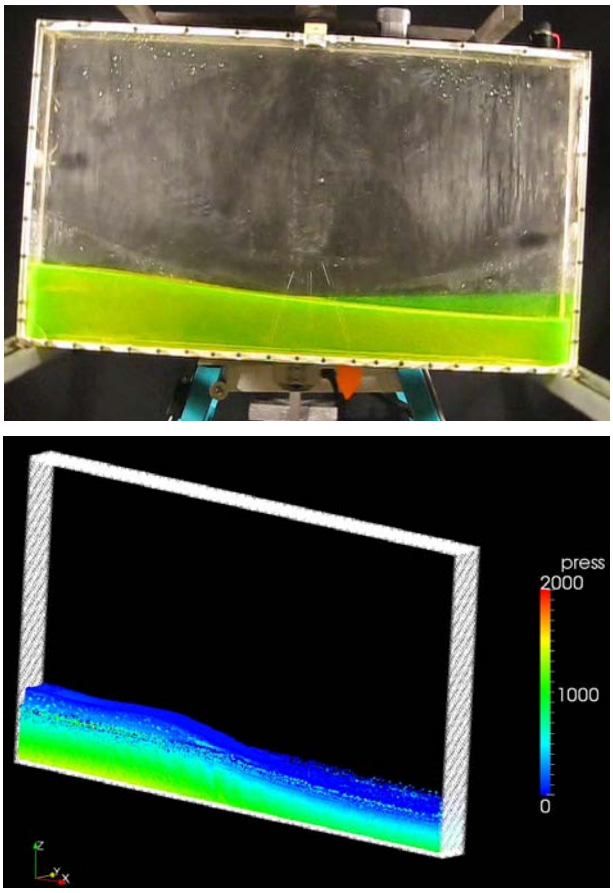

Figure 8 Glycerin, t=9.43s, experiment (top) 3D simulation (bottom)

Bulian, G., Souto-Iglesias, A., Delorme, L., Botia-Vera, E., 2010. "SPH simulation of a tuned liquid damper with angular motion", Journal of Hydraulic Research, Vol. 48 (Extra Issue), pp. 28-39.

Colagrossi, A., Antuono, M., Souto-Iglesias, A., Le Touzé, D., 2011, "Theoretical analysis and numerical verification of the consistency of viscous smoothed-particle-hydrodynamics formulations in simulating free-surface flows". Physical Review E,

Vol. 84, pp.26705+.

Harada, T., Koshizuka, S., Kawaguchi, Y., 2007. Smoothed particle hydrodynamics on GPUs. Proc. of the Computer Graphics International Conference. pp. 63-70.

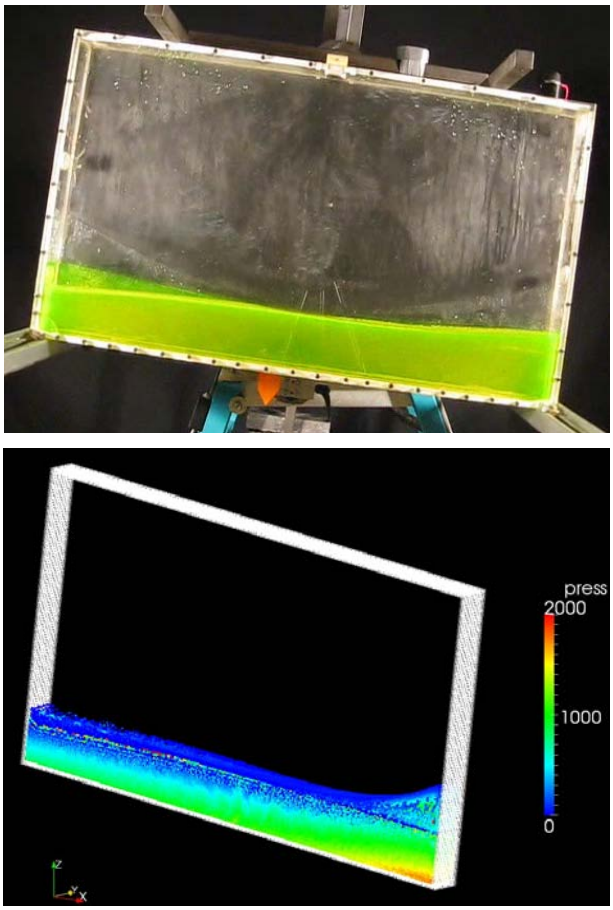

Figure 9 Glycerin, t=10s, experiment (top) 3D simulation (bottom)

Herault, A., Bilotta, G., Dalrymple, R. A., 2010. "SPH on GPU with CUDA". Journal of Hydraulic Research, Vol. 48 (Extra Issue), pp. 74-79.

Hu, X. Y., Adams, N. A., 2006. "Angular-momentum conservative Smoothed Particle Hydrodynamics for incompressible viscous flows", Physics of Fluids, Vol. 18, pp. 702-706.

Landrini, M., Colagrossi, A., Faltinsen, O. M., 2003. Sloshing in 2-D flows by the SPH method. Proceedings of the 8th International Conference on Numerical Ship Hydrodynamics.

Maciá, F., Antuono, M., González, L. M., Colagrossi, A.,, 2011, Theoretical analysis of the no-slip boundary condition enforcement in SPH methods, Progress of Theoretical Physics, Vol., 125, pp. 1091-121.

Monaghan, J. J., 2005. “Smoothed particle hydrodynamics”. Reports on Progress in Physics, Vol. 68, pp. 1703-1759.

Monaghan, J. J., Gingold, R. A., 1983. "Shock simulation by the particle method SPH”. Journal of Computational Physics, Vol. 52, pp. 374-389.

Nam, B.-W., Kim, Y., Kim, D.-W., Kim, Y.-S., 2009. “Experimental and numerical studies on ship motion responses coupled with sloshing in waves”, Journal of Ship Research, Vol. 53, pp 68-82.

Rey-Villaverde, A., Cercos-Pita, J. L., Souto-Iglesias, A., González, L. M., 2011. Particle methods parallel implementations by GP-GPU strategies. Proceedings of the II International Conference on Particle-based Methods - Fundamentals and Applications, PARTICLES 2011.

Souto-Iglesias, A., Botia-Vera, E., Martín, A., Pérez-Arribas, F., Nov. 2011. A set of canonical problems in sloshing. part 0: Experimental setup and data processing. Ocean Engineering, Vol. 38, pp. 1823-1830.

Souto-Iglesias, A., Delorme, L., Rojas, P.L., & Abril, S., 2006, “Liquid moment amplitude assessment in sloshing type problems with SPH”. Ocean Engineering , 33 , 11-12.

Tait, M.J., A.A. El Damatty And N. Isyumov, 2005, “An Investigation of Tuned Liquid Dampers Equipped With Damping Screens under 2D Excitation”. Earthquake Engineering & Structural Dynamics 34 (7): 719-735.